

# Adatom Doping-Enriched Geometric and Electronic Properties of Pristine Graphene: a Method to Modify the Band Gap \*

Ngoc Thanh Thuy Tran<sup>1</sup>, Dipendra Dahal<sup>2</sup>, Godfrey Gumbs<sup>2,3</sup> and Ming-Fa Lin<sup>1</sup>

<sup>1</sup>*Department of Physics, National Cheng Kung University, Tainan 701, Taiwan*

<sup>2</sup>*Department of Physics and Astronomy,  
Hunter College of the City University of New York,  
695 Park Avenue, New York, NY 10065, USA*

<sup>3</sup>*Donostia International Physics Center (DIPC), P de Manuel Lardizabal,  
4, 20018 San Sebastian, Basque Country, Spain*

(Dated: March 8, 2017)

## Abstract

We have investigated the way in which the concentration and distribution of adatoms affect the geometric and electronic properties of graphene. Our calculations were based on the use of first principle under the density functional theory which reveal various types of  $\pi$ -bonding. The energy band structure of this doped graphene material may be explored experimentally by employing angle-resolved photo-emission spectroscopy (ARPES) for electronic band structure measurements and scanning tunneling spectroscopy (STS) for the density-of-states (DOS) both of which have been calculated and reported in this paper. Our calculations show that such adatom doping is responsible for the destruction or appearance of the Dirac cone structure.

PACS numbers: 65.80.*Ck*, 68.65.*Pq*, 72.80.*Vp* and 77.84.*Bw*

---

\* “This paper is dedicated to Professor Lou Massa on the occasion of his Festschrift: A Path through Quantum Crystallography”.

## I. INTRODUCTION

Ever since the successful exfoliation of graphene was achieved, there has been considerable effort both theoretically [1–6] and experimentally [5, 7–9] to exploit its electronic, photonic and mechanical properties. Because of its flexibility, robust strength, heightened intrinsic mobility, high thermal and electrical conductivity and zero band gap at the  $K$  point, linear dispersion and massless fermions, scientists have envisioned potential application for graphene-based electronic devices in the semiconductor industry. Creating pristine graphene in commercial quantities with a specific band gap is a major challenge in its use for nanoelectronic devices. Some of the intriguing properties which have received a great deal of attention include the doping and temperature dependence of plasmon excitations and their energy dispersion dependence on the direction of the wave vector in the Brillouin zone for graphene [10–15], the Klein paradox [16–19], the Veselago lens [19–21], screened impurity potential [22, 23], effect of magnetic field [22] to name just a few.

Placing a graphene layer in close proximity with a substrate such as silicon carbide, copper, hexagonal boron nitride or doping the graphene sheet with a variety of elements such as Hydrogen, Fluorine or Chlorine are some ways for designing the energy band structure of graphene in a specified way. Of these mentioned ways, this paper is primarily concerned with an investigation of the properties of oxygenated graphene, also known as graphene oxide (GO). These GOs, doped by oxygen atom either on one side or both sides, are considered to be useful for a wide variety of device-based applications including supercapacitors [24–27], energy storage [28, 29], sensors [30–32], memristors [28] and water purification [33].

Manufacturing GO commercially at a reasonable cost and in an environmentally favorable manner is another challenge for this material. There exist several methods for producing GO. In 1859, Brodie [34] treated graphite with  $KClO_3$ , an oxidant, to oxidize graphite in  $HNO_3$ . Staudenmaier [35] improved this method later by adding  $H_2SO_4$  to increase the acidity of the mixture. Hummer [36] further developed this method by adding a mixture of  $NaNO_3$ ,  $H_2SO_4$  and  $KMnO_4$ . This latter method is the most widely used because of its shorter reaction time and no  $ClO_3$  emission [37, 38]. Modification of Hummer’s method is the addition of  $H_3PO_4$  with  $H_2SO_4$  in the absence of  $NaNO_3$  and increasing the amount of  $KMnO_4$  [39]. The GOs have been manufactured using a bottom-up method since this

process is simpler and more acceptable from an environmental point of view compared with traditionally top-down methods. Different oxygen concentration may be synthesized by controlling the amount of oxidant  $KMnO_4$ . Also, GO has been manufactured using a bottom-up Tang-lau method since it is simpler and meets environmental standards compared with traditionally top-down methods [40]. The concentration of oxygen may be controlled by regulating the amount of the oxidant compound  $KMnO_4$ [41], or the oxidation time.

Our aim in this paper is to shed light on the electronic properties and geometrical structure of graphene oxide with the use of the Vienna Ab initio Simulation Package (VASP) [42]. The exchange-correlation energy due to the electron-electron interactions is calculated from the Perdew-Burke-Ernzerhof functional under the generalized gradient approximation [43]. The projector-augmented wave pseudopotentials are employed to evaluate the electron-ion interactions [44]. A plane-wave basis set with a maximum plane-wave energy of 500 eV is used for the valence electron wave functions. The convergence criterion for one full relaxation is mainly determined by setting the Hellmann-Feynman forces smaller than  $0.01 \text{ eV}/\text{\AA}$  and the total energy difference less than  $10^{-5} \text{ eV}$ . The first Brillouin zone is sampled in a Gamma scheme by  $30 \times 30 \times 1$  k points for structure relaxations, and then by  $100 \times 100 \times 1$  k points for further calculations on electronic properties. We present our results for different concentrations of C/O. Also, we reported the DOS and energy band structure of GOs to address the critical issue of how to modulate the band gap of graphene. The outline of the rest of our presentation is as follows: In Sec. II, we present and discuss our results for the band structure of GO for various adatom dopings, its geometrical structure and DOS. Section III is devoted to some concluding remarks.

## II. RESULTS AND DISCUSSIONS

The stable adsorption position of O atoms on graphene is determined by comparing the total ground state energies, in which the lower value corresponds to higher stability. Among the bridge-, hollow- and top-sites, our calculations show that the bridge is the most stable one and the top-site is the least stable, in agreement with previous studies [1]. After self-consistent calculations, we found that all the GO systems, with various concentrations and distributions, have stable structures with very slight buckling present as demonstrated in Fig. 1. The main features of geometric structures, including the C-C and C-O bond lengths

are dominated by the O-concentrations, as shown in Table 1. As oxygen atoms are adsorbed on graphene, the C-C bond lengths are dramatically expanded to 1.53 Å for the case of single-side adsorption (50%), which is close to 1.54 Å  $sp^3$  bond length in diamond. The C-C bond lengths gradually recover to that in pristine graphene (1.42 Å) with the decrease of O-concentration, which is consistent with experimental [5] and theoretical [45] results. However, the C-O bond lengths exhibit the opposite dependence. These results indicate that the stronger orbital hybridizations in C-O bonds significantly reduce their lengths and even weaken the  $\sigma$  bonds in C-C bonds. There exists a partial transformation from  $sp^2$  bonds in pristine graphene into  $sp^3$  bonds, in agreement with previous studies [5, 46]. The above-mentioned rich geometric structures lead to diverse electronic properties.

The two-dimensional (2D) band structures along with high symmetry points are useful for examining the electronic properties. When oxygen atoms are adsorbed on graphene, the energy dispersion relations exhibits dramatic changes with the variations in O-concentrations and O-distributions. For monolayer graphene, the  $sp^2$  orbitals of ( $2p_x$ ,  $2p_y$ ,  $2s$ ) possess very strong covalent  $\sigma$ -bonds among the three nearest-neighbor carbon atoms, while the  $2p_z$  orbitals contribute to the weak  $\pi$ -bonds, being associated with the Dirac-cone structure right at the Fermi-level ( $E_F$ ). The  $\sigma$  and  $\sigma^*$  bands form the high-lying electronic structures within a range of  $|E^{c,v}| \geq 3$  eV, in which the extremum energies are at the  $K$  point. The band structures of double-side and single-side adsorptions GOs are shown in Fig. 2 and Fig. 3, respectively. The contributions of O atoms and C atoms passivated with the former are represented by blue and red circles, respectively, in which the dominance is proportional to the circle's radius. Different from pristine graphene, the isotropic Dirac-cone structure near the  $K$  point is destroyed, mainly owing to the serious hybridization between the atomic orbitals of O and passivated C atoms (C atoms bonded O). Instead, there are wide energy gaps (Figs. 2(a)-(c) and Fig. 3(a)) and O-dominated energy bands nearest to  $E_F$  (blue circles). That is, the  $\pi$  bonds due to the neighboring bonds of parallel  $2p_z$  orbitals are replaced by the orbital hybridizations of O-O bonds. As to the strong orbital hybridizations of passivated C atoms and O atoms (red and blue circles dominate simultaneously), their energy bands are located in  $-2.5 \text{ eV} \leq E^v \leq -4 \text{ eV}$ . The deeper  $\sigma$ -bands with  $E^v \leq -4 \text{ eV}$  are formed by the rather strong hybridization of ( $2p_x$ ,  $2p_y$ ,  $2s$ ) orbitals in C-C bonds almost independent of O-adsorption. With the decrease of O-concentrations, the O-dominated bands become narrower and contribute at deeper energy, while the  $\pi$  bands are gradually recovered (Fig.

2(d) and Figs. 3(b)-(f)). This leads to a reduced band gap and the reformation of a distorted Dirac-cone structure.

The energy gap ( $E_g$ ) values are sensitive to changes in the O-concentration and -distribution, as listed in Table 1. They could be divided into three categories, although the dependence on the O-concentration is non-monotonic [2]. The GO systems always have a finite gap for O-concentrations higher than 25%, mainly owing to the sufficiently strong O-O and C-O bonds. In addition,  $E_g$  values are also affected by double-side or single-side adsorptions. Compared to the double-side adsorption of 50% O-concentration, the single-side ones possess larger band gaps, mainly owing to the stronger interactions between O atoms. In the concentration range of 25-4%, the  $E_g$  values decline quickly. This might exhibit small or vanishing gaps related to the reformed distorted Dirac cones Fig. 2(d) and Figs. 3(c)-(d)). The energy gap becomes zero for low concentrations of <4%. This is induced by the fully reformed Dirac cones without energy spacing (Figs. 3(e)-(f)). These feature-rich energy bands of GOs, including the absence and presence of the distorted Dirac-cone structures, and the band gap are expected to be examined by ARPES. By controlling the O-coverage, the band gap of graphene may be significantly adjusted, which opens up the scope for potential use in nanoelectronic devices.

The main characteristics of the band structures are directly reflected in the DOSs, as shown in Fig. 4. The predicted C-O and O-O bonds as a results of oxygen adsorption are clearly viewed by the orbital-projected DOSs. The low-energy DOS is dramatically altered after oxygens are adsorbed on graphene. For pristine graphene, the peaks caused by  $\pi$  and  $\pi^*$  bands due to  $2p_z$ - $2p_z$  bond between C atoms will dominate within the range of  $-2 \text{ eV} \leq |E| \leq 2 \text{ eV}$ . Moreover, a vanishing gapless DOS near  $E_F = 0$  indicates the zero-gap semiconducting behavior. However, for high O-concentrations, the  $\pi$  and  $\pi^*$ -peaks are absent as a result of the strong C-O bond. Instead, there are energy gaps and several O-dominated prominent structures in a wide range of  $E^v \leq -2.5$  to  $E_F$  (Figs. 4.(a)-(c); Figs. 4(e)-(f)). Also, the magnitude of the energy gap depends on the competition between the O-O bonds and the  $\pi$  bonds. Concerning the middle-energy range of  $-2.5 \text{ eV} \leq E^v \leq -4 \text{ eV}$ , the DOSs grow quickly and exhibit prominent peaks due to the C-O bonds. With the decrease in the O-concentration, the  $\pi$  and  $\pi^*$  -peaks are gradually reformed at low energy, while the O-dominated structures present a narrower width and large red shift deeper from

the fermi level (Fig. 4(d); (Figs. 4(g)-(j)). The critical features in DOSs, mainly the finite or vanished energy gaps, the  $\pi$ - and  $\pi^*$ -peaks, the O-dominated special structures, and the (C,O)-dominated prominent peaks can be further verified by STS, giving useful information in determining the oxygen concentration.

### III. CONCLUDING REMARKS

In summary, an important result coming out of our study is that the electronic and geometric structure of graphene may be modified by oxygenation either from one side or from both side. Depending on the distribution and the concentration of the adsorbed oxygen atom, the bond lengths between C-C and C-O change. This leads to the reconstruction of the electronic structure causing the energy band structure to be modified. A finite energy gap emerges as a result of doping and the value of this band gap increases if the level of doping is increased. The emerged energy band gap also depends on single side or double side oxygen adsorption. This behaviour in fact plays an important role in tuning the band gap and modulating the energy band structure of GOs which could be used in designing the on-off feature in semiconductor devices.

- 
- [1] Tran NTT, Lin SY, Lin YT, and Lin MF(2016) Chemical bonding-induced rich electronic properties of oxygen adsorbed few-layer graphenes. *Phys Chem Chem Phys* **18**(5): 4000-4007
  - [2] Tran NTT, Lin SY, Glukhova OE, and Lin MF(2016)  $\pi$ -bonding-dominated energy gaps in graphene oxide. *RSC Adv* **6**(29): 24458-24463
  - [3] Nakada K and Ishii A(2011) Migration of adatom adsorption on graphene using dft calculation. *Solid State Commun* **151**(1): 13-16
  - [4] Brar VW, Decker R, Solowan HM, Wang Y, Maserati L, Chan KT, Lee H, Girit CO, Zettl A, Louie SG(2011) Gate-controlled ionization and screening of cobalt adatoms on a graphene surface. *Nat Phys* **7**(1): 43-47
  - [5] Mkhoyan KA, Contryman AW, Silcox J, Stewart DA, Eda G, Mattevi C, Miller S, and Chhowalla M(2009) Atomic and Electronic Structure of Graphene Oxide. *Nano lett* **9**(3): 1058-1063
  - [6] Lian K-Y, Ji Y-F, Li X-F, Jin M-X, Ding D-J, and Luo Y(2013) Big Bandgap in Highly Reduced Graphene Oxide. *The Jour of Phys Chem C* **117**(12): 6049-6054
  - [7] Zanella I, Fagan SB, Mota R, and Fazzio A(2008) Electronic and magnetic properties of Ti and Fe on graphene. *Jour Phys Chem C* **112**(25): 9163-9167
  - [8] Gao H, Zhou J, Lu M, Fa W, and Chen Y(2010) First-principles study of the IVA group atoms adsorption on graphene. *J Appl Phys* **107**(11): 114311
  - [9] Dai J and Yuan J(2010) Adsorption of molecular oxygen on doped graphene: Atomic, electronic, and magnetic properties. *Phys Rev B* **81**(16): 165414
  - [10] Wunsch B, Stauber T, Sols F and Guinea F(2006) Dynamical polarization of graphene at finite doping. *New Jour of Phys* **8**(12): 318
  - [11] Gumbs G, Horing NJM, Iurov A and Dahal D(2016) Plasmon excitations for encapsulated graphene. *J Phys D: Appl Phys* **49**(22): 225101
  - [12] Gumbs G, Iurov A, and Horing NJM(2015) Nonlocal plasma spectrum of graphene interacting with a thick conductor. *Phys Rev B* **91**(23): 235416
  - [13] Gumbs G, Iurov A, Huang D, and Pan W(2015) Tunable surface plasmon instability leading to emission of radiation. *Journal of Applied Physics* **118**(5): 054303
  - [14] Hwang EH and Sarma SD(2009) Plasmon modes of spatially separated double-layer graphene.

- Phys Rev B **80**(20): 205405
- [15] Hwang EH and Sarma SD(2007) Dielectric function, screening, and plasmons in two-dimensional graphene. Phys Rev B **75**(20): 205418
  - [16] Beenakker CWJ(2008) Andreev reflection and Klein tunneling in graphene. Rev Mod Phys **80**(4): 1337
  - [17] Allain PE and Fuchs JN(2011) Klein tunneling in graphene: optics with massless electrons. Eur Phys J B **83**(3): 301
  - [18] Neto AHC, Guinea F, Peres NMR, Novoselov KS, and Geim AK(2009) The electronic properties of graphene. Rev Mod Phys **81**(1): 109
  - [19] Dahal D, Gumbs G(2017) Effect of energy band gap in graphene on negative refraction through the veselago lens and electron conductance. Journal of Physics and Chemistry of Solids **100**: 83-91
  - [20] Cheianov VV, Falko V and Altshuler BL(2007) The focusing of electron flow and a Veselago lens in graphene pn junctions. Science **315**(5816): 1252-1255
  - [21] Veselago VG(1968) The electrodynamics of substances with simultaneously negative values of  $\epsilon$  and  $\mu$ . Soviet Physics Uspekhi **10**(4): 509
  - [22] Gumbs G, Balassis A, Dahal D, and Glasser ML(2016) Thermal smearing and screening in a strong magnetic field for Dirac materials in comparison with the two dimensional electron liquid. The European Physical Journal B, **89**(10):234
  - [23] Katsnelson MI(2006) Nonlinear screening of charge impurities in graphene. Phys Rev B **74**(20): 201401
  - [24] Karthika P, Rajalakshmi N, and Dhathathreyan KS(2013) Phosphorus-doped exfoliated graphene for supercapacitor electrodes. J Nano sci Nanotechnol **13**(3): 1746-1751
  - [25] Xue Y, Zhu L, Chen H, Qu J and Dai L(2015) Multiscale patterning of graphene oxide and reduced graphene oxide for flexible supercapacitors. Carbon, **92**: 305-310
  - [26] Chen Y, Zhang X, Zhang D, Yu P, and Ma Y(2011) High performance supercapacitors based on reduced graphene oxide in aqueous and ionic liquid electrolytes. Carbon **49**(2): 573-580
  - [27] Gao W, Singh N, Song L, Liu Z, Reddy ALM, Ci L, Vajtai R, Zhang Q, Wei B, and Ajayan PM(2011) Direct laser writing of micro-supercapacitors on hydrated graphite oxide films. Nat Nanotech **6**(8): 496-500
  - [28] Porro S, Accornero E, Pirri CF, and Ricciardi C(2015) Memristive devices based on graphene



- oxide. Carbon **85**: 383-396
- [29] Wang ZL, Xu D, Wang HG, Wu Z, and Zhang XB(2013) In situ fabrication of porous graphene electrodes for high-performance energy storage. ACS Nano **7**(3): 2422-2430
  - [30] Sheng ZH, Zheng XQ, Xu JY, Bao WJ, Wang FB, and Xia XH(2012) Electrochemical sensor based on nitrogen doped graphene: simultaneous determination of ascorbic acid, dopamine and uric acid. Biosens Bioelectron **34**(1): 125-131
  - [31] Veerapandian M, Lee MH, Krishnamoorthy K, and Yun K(2012) Synthesis, characterization and electrochemical properties of functionalized graphene oxide. Carbon **50**(11): 4228-4238
  - [32] Robinson JT, Perkins FK, Snow ES, Wei Z, and Sheehan PE(2008) Reduced graphene oxide molecular sensors. Nano Lett **8**(10): 3137-3140
  - [33] Li F, Jiang X, Zhao J, and Zhang S(2015) Graphene oxide: A promising nanomaterial for energy and environmental applications. Nano Energy **16**: 488-515
  - [34] Brodie B C(1859) On the atomic weight of graphite. Philos Trans R Soc London **149**: 249-259
  - [35] Staudenmaier, L(1898) Verfahren zur darstellung der graphitsure. Eur Jour of Inorg Chem **31**(2): 1481-1487
  - [36] Jr WSH and Offeman RE(1958) Preparation of graphitic oxide. J Am Chem Soc, **80**(6): 1339-1339
  - [37] Poh HL, Sanek F, Ambrosi A, Zhao G, Sofer Z, and Pumera M(2012) Graphenes prepared by Staudenmaier, Hofmann and Hummers methods with consequent thermal exfoliation exhibit very different electrochemical properties. Nanoscale **4**(11): 3515-3522
  - [38] Bai H, Li C, and Shi G(2011) Functional composite materials based on chemically converted graphene. Adv Mat **23**(9): 1089-1115
  - [39] Marcano DC, Kosynkin DV, Berlin JM, Sinitskii A, Sun Z, Slesarev A, Alemany LB, Lu W, and Tour J(2010) Improved synthesis of graphene oxide. ACS Nano **4**(8): 4806-4814
  - [40] Tang L, Li X, Ji R, Teng KS, Tai G, Ye J, Wei C, and Lau SP(2012) Bottom-up synthesis of large-scale graphene oxide nanosheets. J Mat Chem **22**(12): 5676-5683
  - [41] Wu R, Wang Y, Chen L, Huang L, and Chen Y(2015) Control of the oxidation level of graphene oxide for high efficiency polymer solar cells. RSC Adv **5**(61): 49182-49187
  - [42] Kresse G, Furthmüller J(1996) Efficient iterative schemes for ab initio total-energy calculations using a plane-wave basis set. Phys Rev B **54**(16): 11169
  - [43] Perdew J P, Burke K and Ernzerhof M(1996) Generalized gradient approximation made sim-

- ple. Physical review letters **77**(18): 3865
- [44] Blochl PE(1994) Projector augmented-wave method. Phys rev B **50**(24): 17953
- [45] Ito J, Nakamura J, and Natori A(2008) Semiconducting nature of the oxygen-adsorbed graphene sheet. Journal of applied physics **103**(11): 113712
- [46] Hirata M, Gotou T, Horiuchi S, Fujiwara M and Ohba M (2004) Thin-film particles of graphite oxide 1: High-yield synthesis and flexibility of the particles. Carbon, **42**(14): 2929-2937

TABLE I: The optimized C-O bond lengths, C-C bond lengths and energy gap ( $E_g$ ) for various concentrations of GOs.

Adsorption	O:C	%	C-O bond length ( $\text{\AA}$ )	C-C bond length ( $\text{\AA}$ )	$E_g$ (eV)
Double-side	4:8	50	1.44	1.49	3.16
	2:6	33.3	1.47	1.45	1.72
	2:8	25	1.48	1.47	2.44
	2:24	8.3	1.49	1.45	0
Single-side	4:8	50	1.43	1.53	3.56
	5:18	27.8	1.46	1.47	0.88
	3:18	16.7	1.48	1.45	0.64
	2:32	6.3	1.48	1.43	0.36
	1:32	3.1	1.48	1.42	0
	1:50	2	1.48	1.42	0

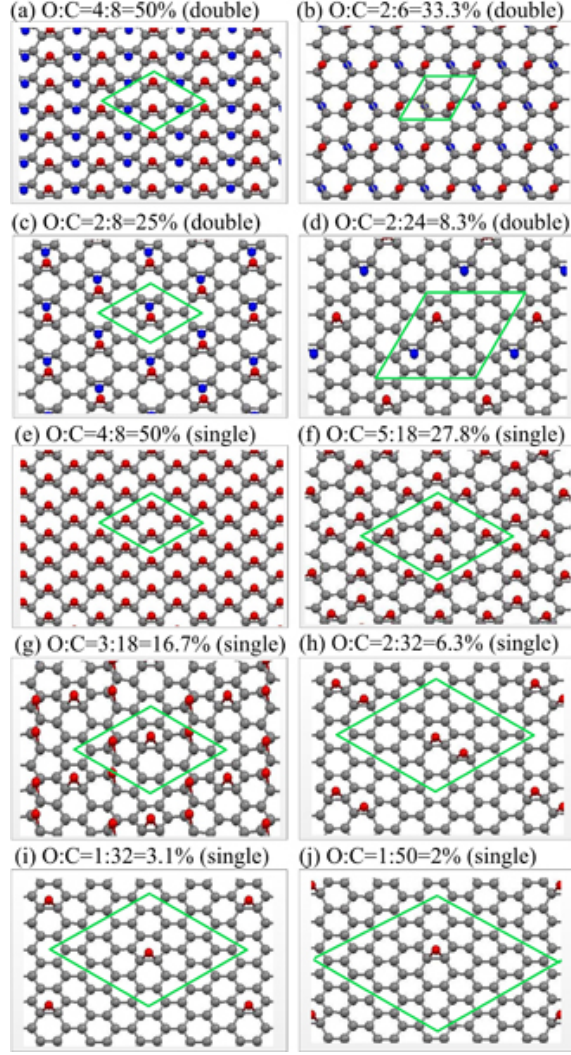


FIG. 1: (Color online) Geometric structures of GOs with various concentrations: double-side adsorptions (a) 50%, (b) 33.3%, (c) 25%, and (d) 8.3%; single-side adsorptions (e) 50%, (f) 27.8%, (g) 16.7%, (h) 6.3%, (i) 3.1%, and (j) 2%. The red and blue atoms, respectively, correspond to O atoms adsorbed on the top and bottom of a graphene layer (gray color).

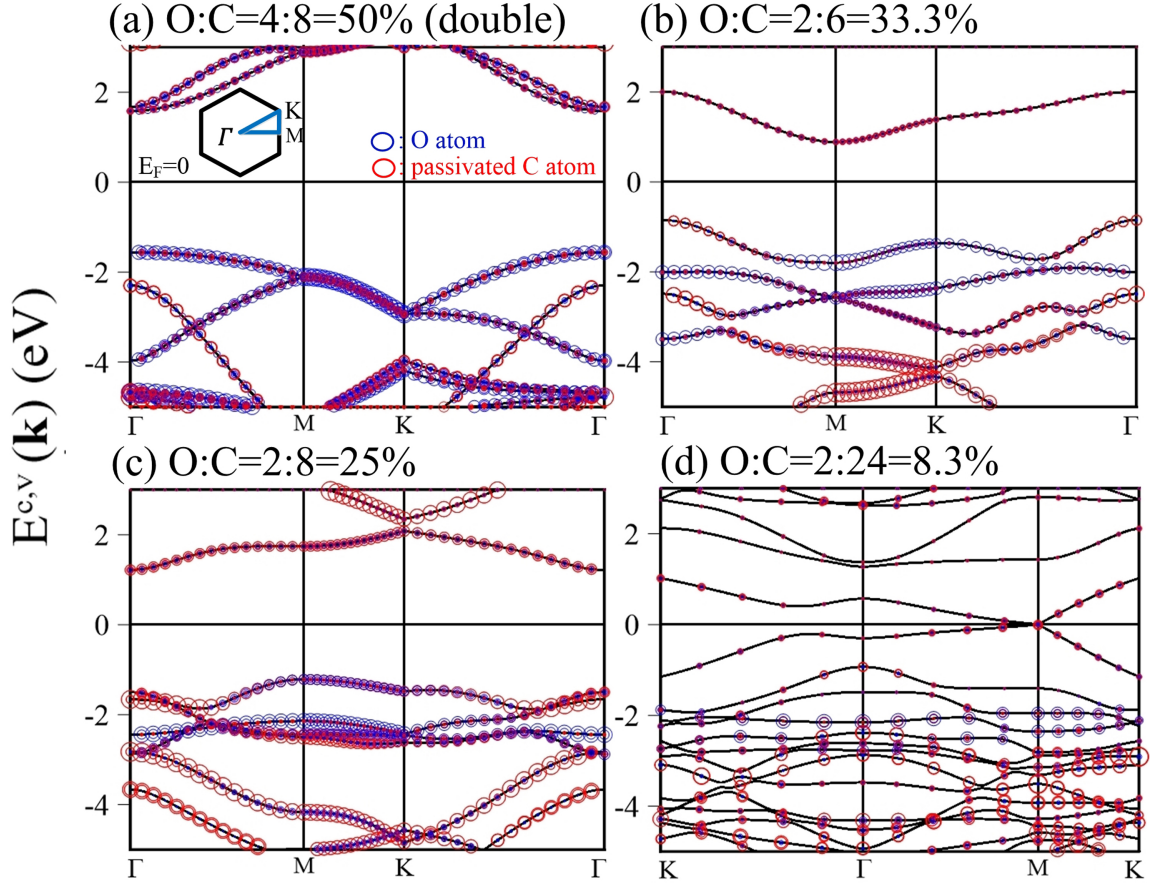


FIG. 2: (Color online) Band structures of double-side adsorbed GOs with various concentrations: (a) 50%, (b) 33.3%, (c) 25%, and (d) 8.3%. Superscripts c and v correspond to the conduction and valence bands, respectively. The red and blue circles, respectively, correspond to the contributions of passivated C atoms and O atoms, in which the dominance is proportional to the radius of circles. Also shown in the inset of (a) is the first Brillouin zone.

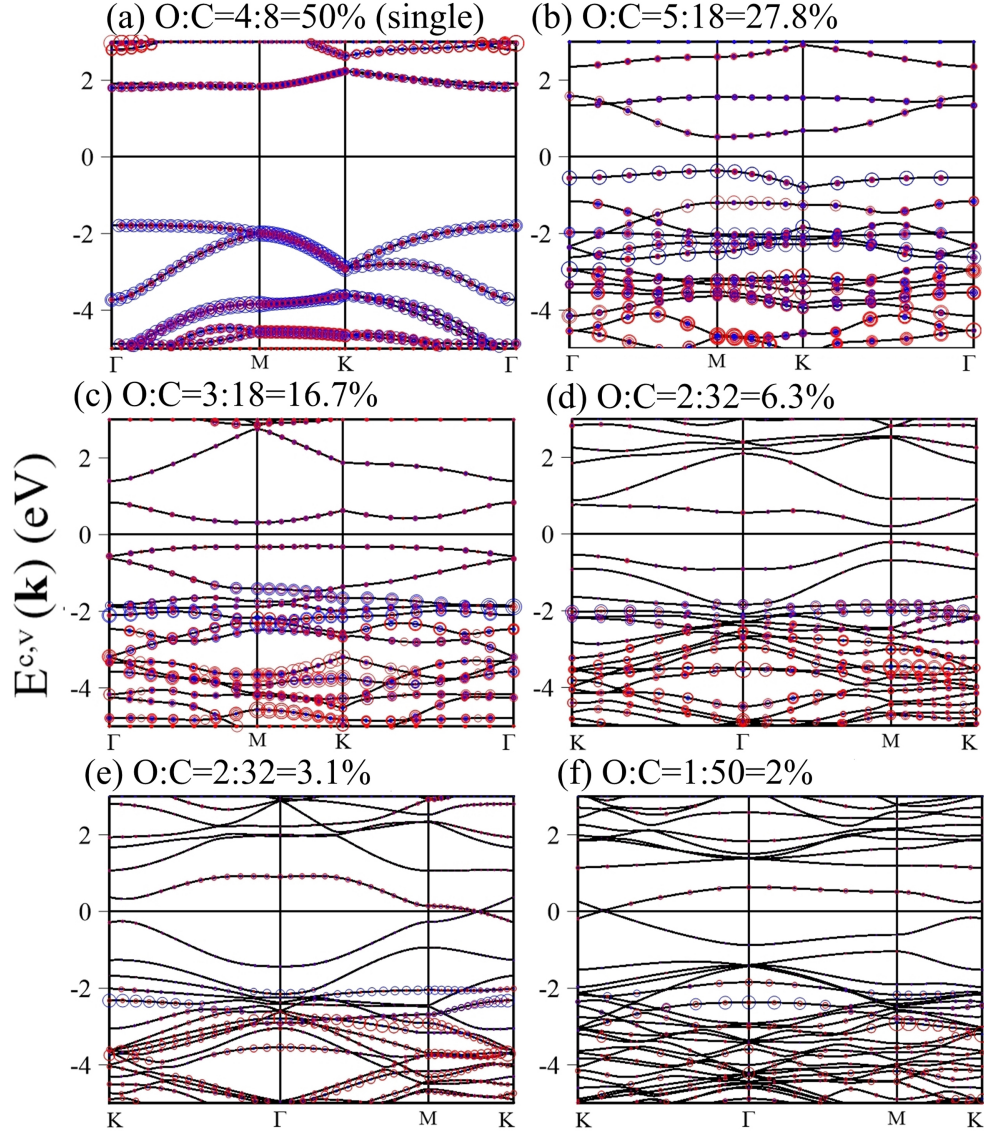


FIG. 3: (Color online) Band structures of single-side adsorbed GOs with various concentrations: (e) 50%, (f) 27.8%, (g) 16.7%, (h) 6.3%, (i) 3.1%, and (j) 2%.

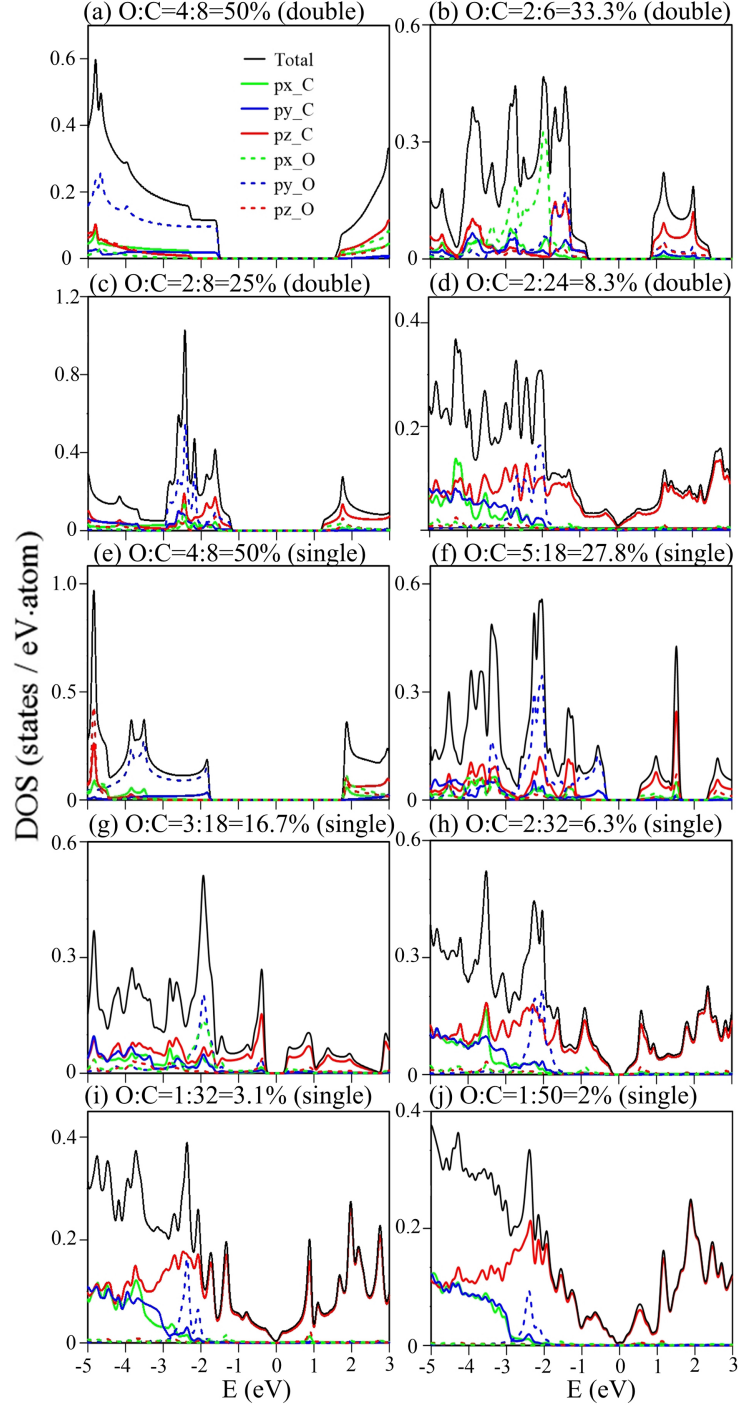


FIG. 4: (Color online) Orbital-projected DOSs of GOs with various O-concentrations:(a) 50%, (b) 33.3%, (c) 25%, (d) 8.3%, (e) 50%, (f) 27.8%, (g) 16.7%, (h) 6.3%, (i) 3.1%, and (j) 2%. Figs. (a)-(d) belong to double-side adsorptions, whereas Figs. (e)-(j) belong to single-side ones.